Microstructure evolution and thermal properties in nanocrystalline Fe during mechanical attrition

ARTICLE *in* PHYSICAL REVIEW B · JANUARY 2001

Impact Factor: 3.74 · DOI: 10.1016/S1359-6454(00)00310-4

3 AUTHORS, INCLUDING:

Howard Sheng
George Mason University
58 PUBLICATIONS **2,779** CITATIONS

Pergamon

Acta mater. 49 (2001) 365–375

Acta MATERIALIA

www.elsevier.com/locate/actamat

MICROSTRUCTURE EVOLUTION AND THERMAL PROPERTIES IN NANOCRYSTALLINE Fe DURING MECHANICAL ATTRITION

Y. H. ZHAO[1]†, H. W. SHENG[2] and K. LU[1]

[1]State Key Laboratory for RSA, Institute of Metal Research, Chinese Academy of Sciences, 72 Wenhua Road, Shenyang 110015, People's Republic of China and [2]Department of Materials Science and Engineering, The Johns-Hopkins University, Baltimore, MD 21218, USA

(Received 17 December 1999; received in revised form 20 June 2000; accepted 20 June 2000)

Abstract—The microstructural evolution and thermal properties of nanocrystalline (nc) Fe during mechanical attrition were investigated by using quantitative X-ray diffraction and thermal analysis techniques. Upon milling of the Fe powders with coarse grains, grain refinement takes place gradually and a steady-state grain size in the nanometer regime is reached after a certain period of milling. With the further milling of the nc Fe within the stage of the steady-state grain size, we observed a grain boundary relaxation process that was manifested by evident decreases in the thermal expansion coefficient and the stored enthalpy, as well as slight decreases in the lattice strain and the Debye–Waller parameter. The grain boundary enthalpy of the nc Fe was estimated, showing a decreasing tendency with the milling time. The present work indicated with clear experimental evidence that the nc materials with the same grain size may exhibit very different properties that depend upon the microstructure of the numerous metastable grain boundaries.

Keywords: Attrition; X-ray diffraction (XRD); Iron; Microstructure; Thermal properties

1. INTRODUCTION

Nanocrystalline (nc) materials have attracted considerable scientific interest in the last decade because of their unusual physical, chemical and mechanical properties that are normally attributed to the ultrafine grains and the numerous grain boundaries (GBs) [1]. However, experimental measurements have shown that the properties of nc materials prepared by means of different approaches can be very different. Various properties showed strong dependence upon the synthesis routes and the processing parameters [2, 3]. The primary reason for this phenomenon might be the fact that some microstructure features are sensitive to the processing parameters, such as porosity, grain size distribution, lattice strain, composition and segregation in GBs, etc. Among these the GB structure is one of the important factors dominating the variation of properties. As the GBs constitute a significant component in the nc materials, it is reasonable to anticipate that for the nc materials with the same grain size and the same chemical composition, properties might change remarkably when the GB structure is altered. However, systematic investigations on the effect of GB structure on the properties of nc materials are rarely reported in the literature. The intrinsic correlation between the GB structure and the properties of nc materials is poorly understood.

As one of the most efficient approaches for preparing nc materials, mechanical attrition by using ball milling has frequently been applied in synthesizing nc metals and alloys, and intermetallics as well [4–8]. The ball milling process, which introduces severe plastic deformation of the milled powders so that fracture and cold-welding of the powders occur, can effectively refine the grains down to the nanometer regime for most metals and alloys. It was found that during the ball milling of metals and alloys, a steady-state grain size (D_{min}) can be reached when the powders were milled for a certain period of time. An extension of milling will not be able to decrease the grain size further. The D_{min} during milling, which was found to scale with the melting points of the metals in some cases [9], is not as yet well understood. It is obvious that the phenomenon is associated with the plastic deformation mechanism and grain size stability of the nc materials. Some explanations have been proposed that D_{min} is correlated with the dislocation (and other defects) activities and recoveries. Nevertheless, no satisfactory explanation has been reached.

In some systems [9–11], it was found that when

† To whom all correspondence should be addressed. Tel.: +86-24-2384-3531; fax: +86-24-2389-1320.

E-mail addresses: yhzhao@imr.ac.cn (Y.H. Zhao), kelu@imr.ac.cn (K. Lu)

1359-6454/01/$20.00
PII: S1359-6454(00)00310-4

D_{min} is reached, further milling will induce reductions of the lattice strain and the stored enthalpy. This might be a hint for a microstructure evolution in the nc materials during milling when the grain size remains constant. Therefore, this phenomenon can be used as a unique opportunity to study the effect of microstructure change (without a grain size change) on properties of the nc materials. The objective of the present work is based on this consideration. In this work, we will study the microstructure evolution and the thermal property changes of nc element Fe during attrition, especially during the stage of D_{min}. Microstructural parameters such as lattice strain and the Debye–Waller parameter, the Debye characteristic temperature as well as thermal properties including the thermal expansion coefficient and the stored enthalpy of the nc Fe samples subjected to different periods of milling, were quantitatively measured. The correlation between the structure and properties was explored. Element Fe was chosen in order to avoid complications due to alloy chemistry and to minimize the contamination from the milling media during the attrition process.

2. EXPERIMENTAL PROCEDURES

2.1. Sample preparation

Fe powders (purity 99.95% and particle size smaller than 200 mesh) were milled in a planetary ball mill with hardened steel balls at ambient temperature. To avoid oxidation, the loaded vial was sealed by an elastic O-ring in dry Ar atmosphere (O_2, H_2<5 ppm) with an over-pressure of about 2 atm. The ball-to-powder weight ratio was 30 to 1 and about 10 g of the Fe powder was charged into the vial. Each mechanical attrition procedure was started with a new dose of the initial powder and was carried out without interruption.

2.2. X-ray diffraction measurements

The quantitative X-ray diffraction (XRD) measurements of the milled Fe powders were carried out on a Rigaku DMAX/2400 X-ray diffractometer. A rotating Cu target was used with a voltage of 40 kV and a current of 100 mA. The X-ray wavelengths $\lambda_{K\alpha 1}$ (=1.54056 Å) and $\lambda_{K\alpha 2}$ (=1.54439 Å) were selected using a ⟨0002⟩ graphite crystal scattering at the goniometer receiving slit. The divergence slit angle, scattering slit angle and receiving slit height were selected as 0.5°, 0.5° and 0.15 mm, respectively. θ–2θ scans with a step size of $2\theta = 0.02°$ and a fixed counting time of 10 s were made for the milled Fe at room temperature (293±1 K). The low-temperature XRD experiments were performed on the same diffractometer with a low-temperature attachment. The milled sample was cooled by liquid N_2 through a metal tube and heated by resistance thread. The temperature (with an accuracy of ±2 K) was detected by a copper–constantan thermo-couple and calibrated by means of a hexagonal-to-orthorhombic phase transition of the NH_4NO_3 sample at 255 K. Only six peaks, reflected from the (110), (200) (211), (220), (310) and (222) planes of the Fe, were scanned at different temperatures (87–293 K) with a step size of $2\theta = 0.02°$ and a counting time of 1 s.

2.3. Thermal and other analyses

Thermal analyses of the milled Fe were performed in a Perkin–Elmer differential scanning calorimeter (DSC-7) with a sensitivity of 0.04 mJ/s for energy measurements. The milled Fe powders were sealed in Al pans and heated in a flowing Ar atmosphere at a constant heating rate of 10 K/min. The temperature for the DSC measurements was calibrated with pure In, Zn standard samples, with an accuracy of better than ±0.2 K. Transmission electron microscopy (TEM) observations were conducted on a Philips EM 420 microscope operated at 100 kV. The milled Fe powders, directly supported by Cu grids which were coated with C films, are used for TEM observations. Compositions of the milled samples were examined by means of wet chemical analysis and O content was detected by LECO TC-436 O/N analysis.

3. RESULTS

3.1. Microstructure evolution

3.1.1. Grain size and lattice strain. Figure 1 shows the typical XRD patterns of the Fe samples

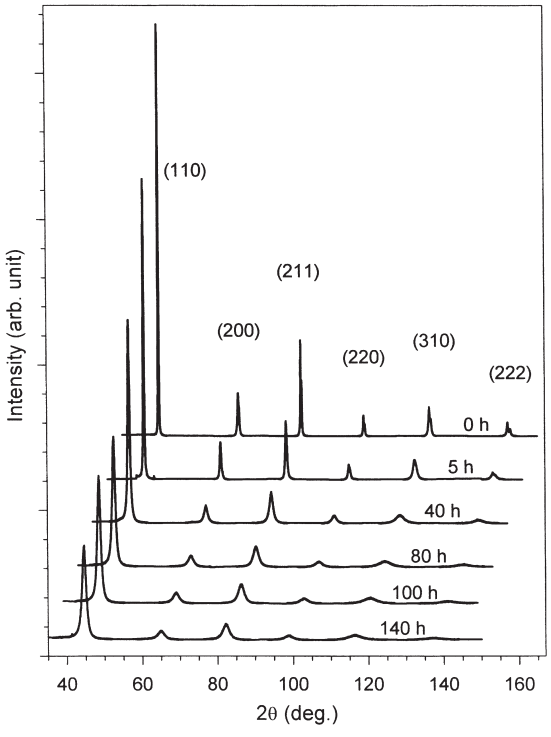

Fig. 1. The XRD lines of the milled Fe samples with different milling times (as indicated). The upper line moves 5° towards the high diffraction angle compared to the line below.

subjected to different periods of milling. It can be seen that, with the milling proceeding, the reflection peak intensities of the milled samples are decreased and the peaks are significantly broadened, suggesting that a large amount of defects were introduced into the samples by mechanical attrition. Moreover, the relative peak intensities of the milled samples are found to be comparable to the standard values of Fe in JCPDS cards [12], indicating that there is no evident texture induced into the samples during attrition.

The broadening of the experimental reflection peaks of the b.c.c. structure Fe is caused by the small size of the diffracting grains, the lattice strain and the instrumental broadening. Often, sufficient information about the changes in grain size and lattice strain can be gained from the integrated width of the peaks, which must assume a model for the functional dependence of the grain size, lattice strain and instrumental broadening on the diffraction angle. The instrumental broadening profiles, determined by means of the SiO_2 reference sample in the present work, are revealed to be Gaussian function. The experimental Bragg reflections with polarization factor correction, fitted by the Pseudo–Voigt function (a linear combination of the Lorentzian and Gaussian functions) [13], can be mainly approximated by a Lorentzian function, as shown in Fig. 2(a). Therefore, one can get the physical profile of the milled Fe, which is the convolution of size broadening with the strain broadening profile, by removing the instrumental broadening effect from the measured intensity profile. Both theory and experiment support the approximation of size broadening profiles by a Lorentzian function [14] and strain broadening by a Gaussian function [15]. Hence, the grain size and the lattice strain of the sample can be calculated from the integral width of the physical broadening profile β_{hkl} by [15]:

$$\frac{\beta_{hkl}^2}{tg^2\theta_{hkl}} = \frac{\lambda\beta_{hkl}}{D_{hkl}tg\theta_{hkl}\sin\theta_{hkl}} + 16\langle\varepsilon_{hkl}^2\rangle^{1/2}, \qquad (1)$$

where λ is the wavelength of Cu $K_{\alpha 1}$ irradiation, and D_{hkl} and $\langle\varepsilon_{hkl}^2\rangle^{1/2}$ represent the thickness and the mean magnitude of the lattice strain of the grains in the $\langle hkl\rangle$ direction, respectively. By performing a least-square fit to $\beta_{hkl}^2/tg^2\theta_{hkl}$ plotted against $\lambda\beta_{hkl}/(tg\theta_{hkl}\sin\theta_{hkl})$ for all of the measured peaks of a sample, we are able to determine the mean grain size D and the mean lattice strain $\langle\varepsilon^2\rangle^{1/2}$. Standard linear regression techniques provide an estimate for the uncertainty in the parameters from the error in the fit [16]. From the pairs of (110)–(220) Bragg reflections, the grain size (D_{110}) and lattice strain ($\langle\varepsilon_{100}^2\rangle^{1/2}$) along the $\langle 110\rangle$ direction of the milled Fe samples can be obtained.

The D, $\langle\varepsilon^2\rangle^{1/2}$, D_{110} and $\langle\varepsilon_{110}^2\rangle^{1/2}$ of the milled samples are plotted in Fig. 2(b). D is found to decrease gradually from 43±8 (0 h) to 8±1 nm (60 h), and remain unchanged at a steady-state value (about 8 nm) with extensive milling. The $D_{\min}$ of the milled Fe in the literature was reported to be 8 nm [17], 9.9 mn [18] and 13 nm [19], which is close to the present value. From Fig. 2(b), one can see that $\langle\varepsilon^2\rangle^{1/2}$ increases from about 0 to 0.65±0.05% (80 h) and then decreases slightly to 0.56±0.05% (140 h) with the extension of milling. In the literature, the maximum $\langle\varepsilon^2\rangle^{1/2}$ of the milled Fe was measured to be 0.4–0.6% [19, 20], agreeing with the present value. The D values estimated from XRD peak broadening were further confirmed by TEM observations (Section 3.1.3), as indicated in Fig. 2(b).

According to Fig. 2(b), it is clear that the difference between D_{110} and D decreases with increasing milling time (t_m), and when t_m>40 h, D_{110} and D are approximately equal, suggesting the grain of the milled nc Fe samples becomes equiaxial with further milling. Moreover, the values of $\langle\varepsilon_{110}^2\rangle^{1/2}$ are very close to those of $\langle\varepsilon^2\rangle^{1/2}$ during the milling process. However, lattice strains are found to exhibit significantly anisotropy behaviour in f.c.c. nc Pd made by means of consolidation of ultrafine particles [21], nc Cu by the severe plastic deformation method [22] and by mechanical attrition [23]: the lattice strains along the $\langle 200\rangle$ direction are much larger than those along the $\langle 111\rangle$ direction. For the nc-Se samples (h.c.p.) made by crystallizing from the as-quenched amorphous solid [24], the strain in the $\langle 100\rangle$ direction is larger than that in the $\langle 104\rangle$ direction. The different deformation mechanisms of different crystalline systems may be

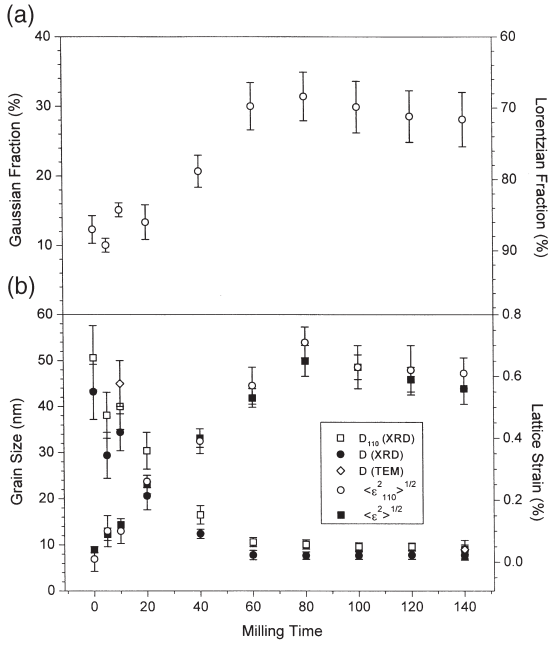

Fig. 2. (a) Variation of the Gaussian/Lorentzian fraction of Bragg reflections of XRD patterns for the milled Fe against the milling time. (b) Milling time dependence of the mean grain size D and mean lattice strain $\langle\varepsilon^2\rangle^{1/2}$, the grain size ($D_{110}$) and lattice strain ($\langle\varepsilon_{100}^2\rangle^{1/2}$) along the $\langle 110\rangle$ direction of the milled Fe samples.

responsible for these different observations of lattice strains.

3.1.2. Debye–Waller parameter and characteristic temperature. The low-temperature XRD experiments of the milled Fe powders were performed in order to obtain more atomic structure information, such as the Debye–Waller parameter (DWP) and the Debye characteristic temperature (Θ_D). The DWP $B(T)$ can be obtained from the XRD patterns by using the Warren method [25], which relies on the sample being free of texture and can be expressed as:

$$\ln(\phi_{hkl}/m_{hkl}) = -2B(T)\sin^2\theta_{hkl}/\lambda^2 + J, \qquad (2)$$

where ϕ_{hkl} is the integrated intensity of (hkl) reflection divided by the Lorentzian, polarization factors and structural factor, m_{hkl} is the multiplicity factor, θ_{hkl} represents the centroid peak position, and J is a constant scaled with the incident intensity. $B(T)$ contains the contributions from static lattice distortions B_S which are temperature-independent and from the thermal vibrations of atoms B_T. For a bulk crystal, the temperature dependence of B_T, is known to be well predicted by the Debye approximation, particularly at low temperatures [25], and $B(T)$ can be represented by:

$$B(T) = B_S + 6h^2F(x)/mk_B\Theta_D, \qquad (3)$$

where h, m and k_B are the Planck constant, the atomic mass and the Boltzmann constant, respectively;

$$x = \Theta_D/T \text{ and } F(x) = \frac{1}{4} + 1/x^2\int_0^x \xi\, d\xi/[\exp(\xi)-1].$$

According to equation (2) we plotted $\ln(\phi_{hkl}/m_{hkl})$ against τ^2 ($\tau = 4\pi\sin\theta/\lambda$) for the milled Fe samples at different temperatures in order to obtain the temperature dependence of $B(T)$. Figure 3(a) shows the plots for the different milled Fe samples at 293 K and Fig. 3(b) gives the plots of the Fe sample with $t_m = 140$ h at different temperatures (87–293 K). For each set of data, a straight line can be drawn by the least-square fitting, from which $B(T)$ is obtained. From Fig. 3(a), one may see that with an increase in the milling time from 0 to 80 h, the absolute value of the slope of the fitting straight line increases, i.e. the DWP at 293 K, $B(293)$, increases, while $B(293)$ decreases when t_m>80 h [see Fig. 5(a)]. The dashed line in Fig. 3(a) is the fitting to the literature value [26]. From Fig. 3(b), one can see that $B(T)$ increases at higher temperatures.

Figure 4 plots the temperature dependence of $B(T)$ for the milled Fe samples. It is clear that $B(T)$ varies significantly with t_m and the temperature. In terms of equation (3), $B(T)$–T can be fitted by adjusting Θ_D and B_S. The solid lines in Fig. 4 show the Debye model fitting to the measured data, and the dashed line shows the fitting to the literature data [26]. The parameters Θ_D and B_S obtained from the fitting results are plotted in Figs 5(a) and (b). B_S is found to increase evidently from 0.10±0.03 (0 h) to 0.25±0.04 Å^2 (80 h) and decrease slightly to 0.21±0.03 Å^2 (140 h). The B_S value for the initial sample is close to the value of 0.075 Å^2 obtained by fitting the literature $B(T)$ values

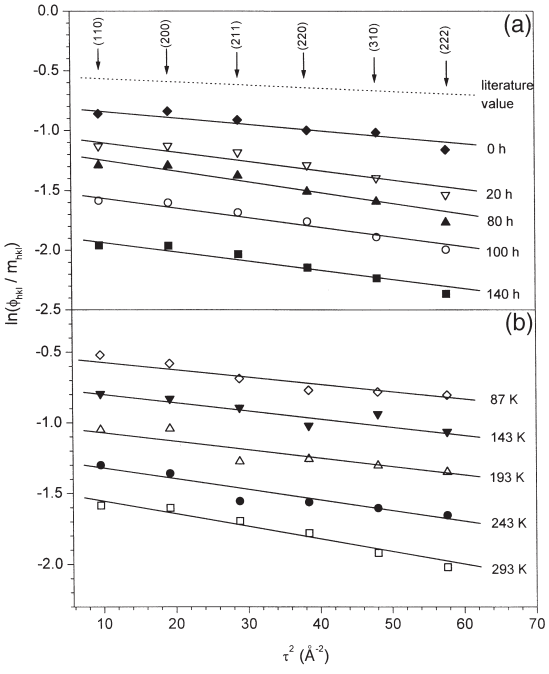

Fig. 3. The logarithm of integrated peak intensities divided by the appropriate multiplicity factors, Lorentzian, polarization factors and structural factors for the different milled Fe samples at 293 K (a), and the sample with t_m = 140 h at different temperatures (b). The solid lines represent the least-square fitting to the measured data, and the dashed line is the fitting to the literature value [26].

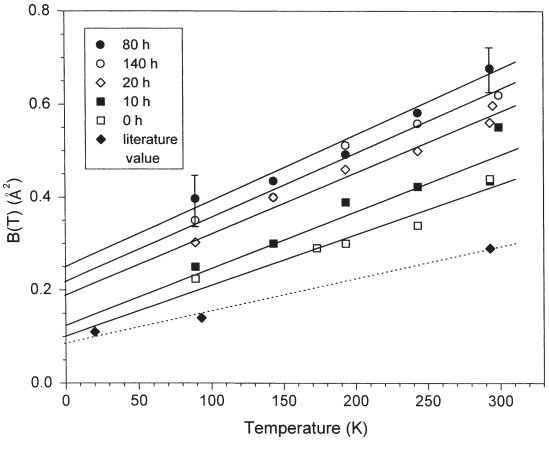

Fig. 4. The DWP $B(T)$ plotted against temperature for different milled nc Fe samples. The solid lines are the Debye model fitting of the measured data, and the dashed line represents the fitting of the literature data [26].

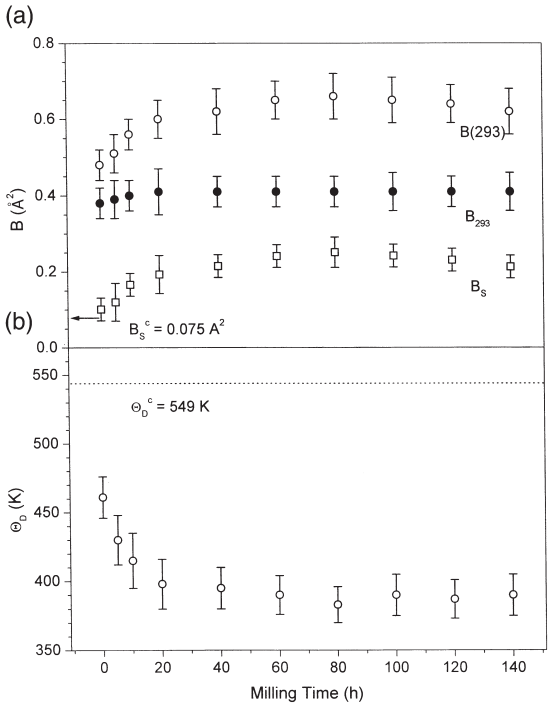

Fig. 5. (a) Plots of the DWP $B(293)$, the static (B_S) and the thermal (B_{293}) DWPs at 293 K vs. the milling time. (b) Plots of the Debye temperature Θ_D for the milled Fe vs. t_m.

for crystal Fe [26]. As $B(T)$ is composed of B_S and B_T, we derived B_T at 293 K, B_{293}, based on the measured data of $B(293)$ and B_S. As shown in Fig. 5(a), B_{293} remains virtually constant during the milling process. Θ_D is observed to drop from 461±15 (0 h) to 383±13 K (80 h) and remains stable within the error bar with further milling [Fig. 5(b)]. The value of the Debye temperature for the unmilled sample is much smaller compared to that obtained by fitting the literature value for the crystal Fe ($\Theta_D^c = 549$ K) [26], which may be caused by the structural imperfections of the unmilled sample.

DWP and Θ_D of the milled nc materials are rarely reported in the literature. However, some investigations have indicated that ultrafine nc metal particles prepared by gas condensation [27–35] and bulk nc Se by crytallization [36] possess the larger B_S and depressed Θ_D compared to those of the corresponding bulk crystals. Evidently, the observed enhanced DWP and decreased Θ_D of the milled Fe samples at the stage of grain refinement agree with the literature.

3.1.3. TEM and composition analyses. TEM analysis was employed to obtain further information about the morphology and microstructure of the milled Fe powders. From TEM observations, we found that the milled particles are sphere- or ellipsoid-shaped, and their sizes range from a few micrometers to submicrometers. The milled particles are polycrystalline, composed of a large amount of manometer-sized grains. Figures 6(a) and (b) show the dark-field images and the diffraction patterns of as-milled Fe particles after 10 and 140 h of milling, respectively. One can see that at the beginning of the milling the distribution of grain size is rather inhomo-

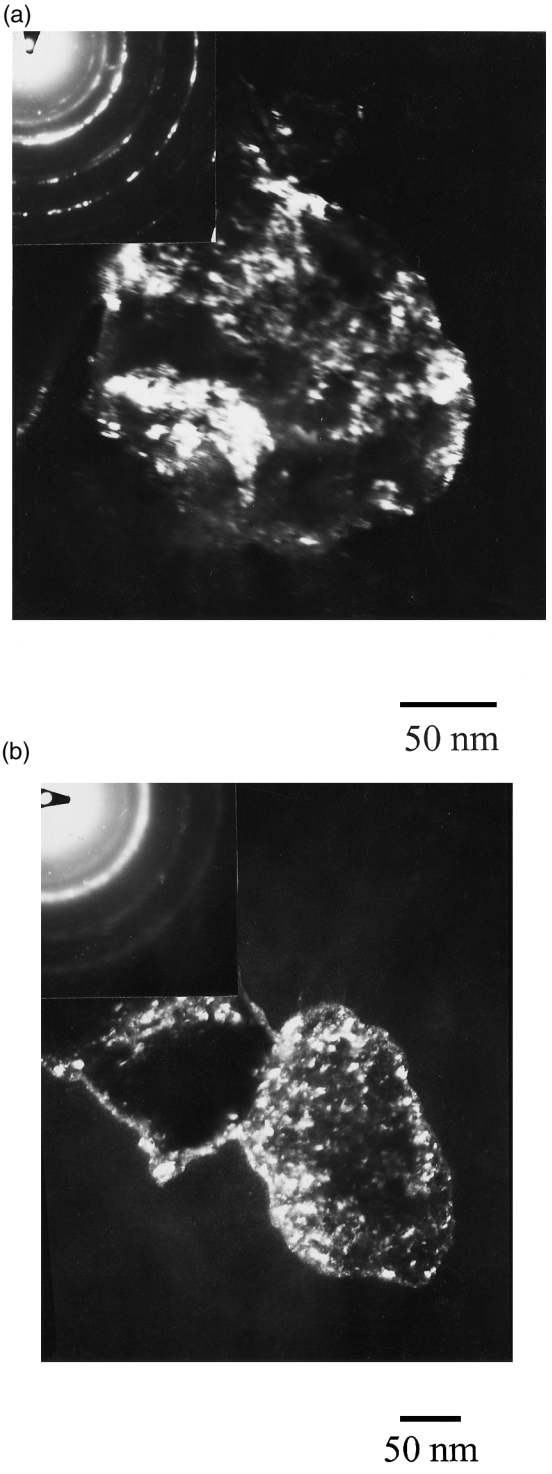

Fig. 6. TEM dark-field images for the nc Fe after 10 h (a) and 140 h (b) of milling. The insets show the corresponding diffraction patterns.

geneous, meaning that partial deformation takes place in the milled powders by attrition. At the end of the milling process (t_m = 140 h), however, the grain size distribution is relatively narrow, and the corresponding diffraction pattern [Fig. 6(b)] shows that the orientation of neighboring crystals is completely random. The *D* value, as estimated from TEM pictures, is about 9 nm when t_m = 140 h, being in good agreement with the value obtained from the broadening of XRD peaks, as plotted in Fig. 2(b).

Since the Fe powders underwent a long period of milling, contamination from milling media and atmosphere was inevitable. Wet chemical analysis shows that the content of Cr reaches a maximum of 0.05 wt.% after 140 h of milling, suggesting that the contamination from the milling media is minor. The O analysis indicates less than 1 at.% O exists in the dispersion milled for 140 h.

3.2. Thermal properties

3.2.1. Thermal expansion coefficient. Values of the lattice parameter *a* for the milled nc Fe at various temperatures (87–293 K) were calculated from the intensity centroid positions of the XRD lines by the weighted least-square method in order to minimize the calculation error. The intensity centroid positions were calibrated by an external standard method using a pure Si polycrystal to minimize the systemic error. A detailed procedure for this determination was described in [24]. Figure 7(a) shows the measured *a* as a function of temperature for the milled nc Fe samples. It is obvious that *a* increases in an approximate linear relation with temperature in the measured temperature range. The average linear expansion coefficient for these nc samples, α_L^{nc}, may be determined from the average slopes of the least-square fitting lines of the measured *a* in the measured temperature range, as shown in Fig. 7(b). It is clear that with increasing t_m from 0 to 80 h, α_L^{nc} increases monotonically from about $(0.8\pm0.2)\times10^{-5}$ up to $(2.5\pm0.4)\times10^{-5}$/K and drops down to $(1.2\pm0.4)\times10^{-5}$/K (140 h). Dilatometric measurements showed that the thermal expansion coefficient of the conventional polycrystalline Fe, α_L^c, is about 1.1×10^{-5}/K at 300 K [37], which is close to the value of the unmilled Fe sample. In the literature, very few investigations were performed on the thermal expansion of the milled nc materials; most of the studies were focused on α_L^{nc} of nc materials synthesized by gas condensation and crystallization methods, such as nc Se [36], Cu [38], Pd [39] and Ni–P [40], etc. The α_L^{nc} of these nc materials are found to be larger than those of the corresponding coarse-grained polycrystalline. It is evident that the increased α_L^{nc} of the milled nc Fe when $t_m<80$ h agrees well with the literature. The decreased α_L^{nc} at the latter stage of milling will be discussed in Section 4.2.1.

3.2.2. The stored enthalpy. Figure 8 shows the DSC scans (320–773 K) for the milled Fe samples with different stages of milling. It can be seen that,

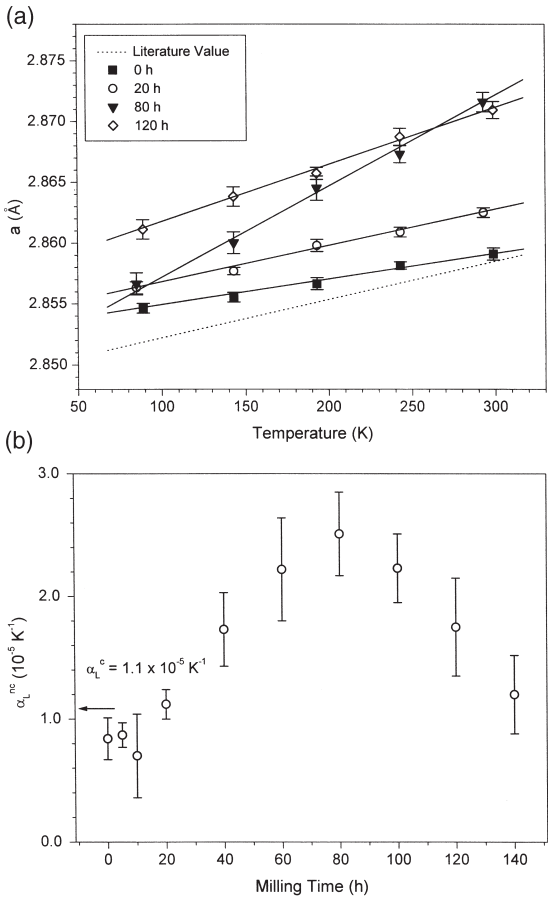

Fig. 7. (a) Plots of the temperature dependence of the lattice parameter *a* of the milled nc Fe. The solid lines are the least-square fitting to the measured data, and the dashed line represents the fitting to the literature values [37]. (b) Plots of the milling time dependence of the linear thermal expansion coefficient α_L^{nc} for nc Fe samples.

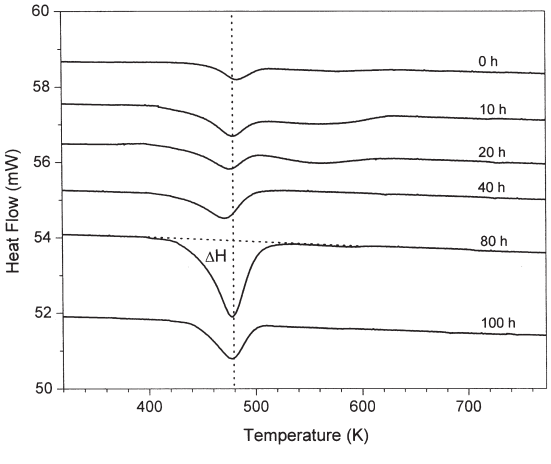

Fig. 8. DSC scans at the heat rate of 10 K/min for the milled nc Fe samples. Integration of the signal deviating from the baseline gives the stored enthalpy ΔH.

when $t_m \leq 20$ h, an exothermic peak with a long tail appears in the DSC curves, but when $t_m \geq 40$ h, the long tail fades away. Moreover, the exothermic peak in the DSC lines was found to become sharper first (0–80 h) and then turn broadened during the milling process, while the peak position is nearly the same, as indicated in Fig. 8. In the literature, it was found that the DSC exothermic peak of the milled nc Ni becomes sharper with the milling process because of the recovery and grain growth of the milled powders [9]. By integrating the area up the exothermic peak (for the samples when $t_m \leq 20$ h, the integration includes the part of the long tail), we obtained the stored enthalpy, ΔH, as shown in Fig. 9. ΔH is observed to possess a maximum value at 80 h (0.82±0.15 kJ/mol) and decreases largely with the extended milling (ΔH = 0.46±0.10 kJ/mol when t_m = 140 *h*). Similar variations of ΔH were found in the milled nc Ni [9], AlRu, Ru [10] and W [11], etc.

XRD analysis was used to examine the microstructural changes of the milled Fe after DSC annealing. The XRD conditions for the as-annealed samples are the same as those for the as-milled ones. Figures 10(a)–(d) show the plots of the Gaussian component of the Bragg reflection, D, $\langle \varepsilon^2 \rangle^{1/2}$ and $B(293)$ of both as-annealed and as-milled Fe samples against t_m. It is clear that, after DSC annealing, the Gaussian fraction, $\langle \varepsilon^2 \rangle^{1/2}$ and $B(293)$ are decreased remarkably, suggesting that the defects were recovered after annealing. The grain growth only takes place at the early stage of milling, which corresponds to the long tail in DSC curves; when $t_m > 20$ h, a very slight increment in D was observed compared to that of the as-milled samples. The absence of grain growth was further confirmed by TEM analysis. This observation means that the exothermic peak in the DSC curves when $t_m > 20$ h is primary originated from a relaxation of the defects with a minor contribution from grain growth, while in the literature, evident grain growth and strain release were observed in the milled f.c.c. metals (Ni and Ru) during DSC runs [9, 10]. The stable grain size in the milled nc Fe might be attributed to either the contamination from the ball-milling process or the large lattice strain that hinder the grain growth process [41, 42]. A small GB enthalpy might also be partially responsible for the stable grain size, as will be discussed in the next section.

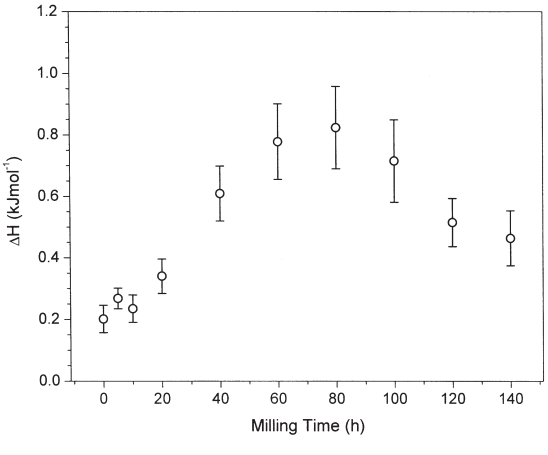

Fig. 9. The stored enthalpy ΔH in ball-milled nc Fe against the milling time.

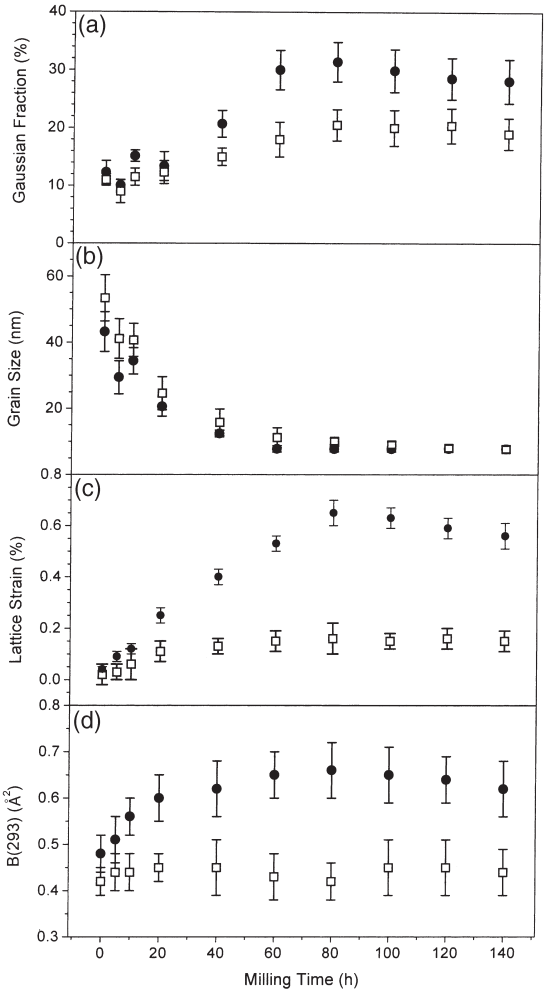

Fig. 10. The Gaussian component (a), the mean grain size (b), the mean lattice strain (c) and the DWP $B(293)$ (d) for the as-annealed (open square) and as-milled (solid circle) Fe samples vs. the milling time.

4. DISCUSSION

From the above analyses, it is clear that the mechanical attrition process of Fe powders can be separated into two stages: grain refinement and grain steady state. In the former case, a large amount of defects (such as GBs, dislocations and point defects, etc.) were introduced into the samples, causing the increases in $\langle \varepsilon^2 \rangle^{1/2}$, B (B_S), α_L^{nc} and ΔH, as well as the decrease in Θ_D. In the latter case, however, slight decreases in the structural parameters ($\langle \varepsilon^2 \rangle^{1/2}$ and B_S) and evident drops in thermal properties (α_L^{nc} and ΔH) were observed, which means that microstructural

variation of the milled Fe samples occurred, even though D remains constant.

Usually, the nc materials can be considered simply to consist of two components: ultrafine grains with sizes in the nanometer range and a numerous amount of GBs. The atoms on the GBs may contribute to the Bragg reflections when they are associated with the crystallite lattice. Therefore, the observed information about the structure and the properties is from both the interiors and boundaries of the grains. The crystallite structures of the nc materials are usually considered as the same as that of the coarse-grained polycrystalline. The observed variations in the structural parameters and the thermal properties of the milled nc Fe within the state of D_{min} may suggest structure evolution in the GBs.

4.1. Microstructural evolution

For milled samples subjected to severe plastic deformation, dislocations are the main defects besides GBs, of which density ρ can be represented in terms of D and $\langle\varepsilon^2\rangle^{1/2}$ by [43,44]:

$$\rho(\rho_D\rho_S)^{1/2} = 2\sqrt{3}\langle\varepsilon^2\rangle^{1/2}/(Db), \tag{4}$$

where b is the Burgers vector of dislocations, and equals 0.24824 nm for Fe. The calculated dislocation density of the as-milled (ρ_{milled}) and as-annealed Fe samples ($\rho_{annealed}$) are listed in Table 1. It is clearly seen that ρ_{milled} increases from about 0.01×10^{16} to $1.17\times10^{16}/m^2$ with increasing t_m from 0 to 80 h, and then decreases slightly to $1.02\times10^{16}/m^2$ (140 h) with further milling. The maximum ρ_{milled} in present work is comparable to the dislocation densities limit in metal achieved by plastic deformation ($10^{13}/m^2$ for screw dislocations, $10^{16}/m^2$ for edge dislocations) [6,7]. For the milled nc Fe in [20], the maximum ρ determined by the Fourier method is about $1.65\times10^{16}/m^2$. Usually, in conventional polycrystalline materials, the GBs are thought to be barriers to the dislocations motion, therefore, the slight decrease in ρ_{milled} within the D_{min} stage indicates a softening of the GBs. When the GBs have turned soft or relaxed, the amount of the dislocations piled up near the GBs will be decreased.

Based on the diffraction theory [45], B_S is due to the presence of defects with short-ranged displacement fields, such as point defects, etc. An enhancement in B_S at the stage of grain refinement means that a large amount of short-ranged defects were introduced into the samples. However, the slight decrease in B_S at the stage of steady-state grain size suggests a recovery of the short-ranged defects, which may be caused by the relaxation of GBs, as verified in Section 4.2. The Θ_D of material is a fundamentally physical parameter designating the cohesion of atoms. At the stage of grain refinement, the depression of Θ_D in nc Fe implies a decrease in the cohesion of atoms in the nm-sized crystallites, which agrees with the measured milling time dependence of $\langle\varepsilon^2\rangle^{1/2}$ and B_S. In fact, the observed larger B_S and $\langle\varepsilon^2\rangle^{1/2}$ in the nc Fe sample with smaller grains may result in a decrease in the elastic modules and hence a depression in Θ_D.

4.2. Thermal properties of GBs

4.2.1. Thermal expansion coefficient of GBs. It is normally considered that the GBs have an enhanced thermal expansion coefficient compared to that of the crystal lattice due to their excess volume, although the amounts of enhancement are found to vary in different investigations [21, 27, 46, 47]. By describing the nc material as a two-component system with crystallites and GBs, α_L^{nc} can be estimated by approximate scaling of the GBs' contribution:

$$\alpha_L^{nc} = F_{GBs}\alpha_L^{GBs} + (1-F_{GBs})\alpha_L^{c}, \tag{5}$$

where F_{GBs} is the volume fraction of GBs, $F_{GBs} = 3\delta/D$ (δ is a constant relative to the GBs' thickness), α_L^{GBs} and α_L^{c} are linear thermal expansion coefficients for GBs and the crystallites, respectively. From equation (5) we may get:

$$\Delta\alpha_L = \alpha_L^{nc} - \alpha_L^{c} = (\alpha_L^{GBs} - \alpha_L^{c})\frac{\delta}{D}. \tag{6}$$

Table 1. A list of the mean dislocation density of the as-milled (ρ_{milled}) and as-annealed ($\rho_{annealed}$) Fe samples, the elastic energy release of dislocations (ΔE_{DS}), the GB enthalpy release (ΔE_{GBs}), and the GB enthalpy release per area ($\Delta\gamma_{GBs}$) for the milled Fe samples

Milling time (h)	ρ_{milled} ($10^{16}/m^2$)	$\rho_{annealed}$ ($10^{16}/m^2$)	ΔE_{DS} (10^{-2} kJ/mol)	ΔE_{GBs} (10^{-2} kJ/mol)	$\Delta\gamma_{GBs}$ (J/m^2)
0	0.01	0.00	0.06	20.05	–
5	0.04	0.02	0.21	25.13	–
10	0.05	0.03	0.11	22.34	–
20	0.17	0.07	1.07	32.39	–
40	0.45	0.14	3.16	57.52	0.16
60	0.95	0.19	6.98	70.37	0.13
80	1.17	0.22	8.93	73.38	0.13
100	1.14	0.23	8.56	63.11	0.11
120	1.05	0.27	7.71	44.34	0.08
140	1.02	0.27	7.25	39.09	0.07

If both α_L^{GBs} and α_L^c are independent of D, one may expect that a plot of $\Delta\alpha_L$ vs. D^{-1} should yield a straight line with a slope of $\delta(\alpha_L^{GBs}-\alpha_L^c)$.

Figure 11 shows a plot of $\Delta\alpha_L/\alpha_L^c$ vs. D^{-1} using the experimental data for the nc Fe and taking $\alpha_L^c = 0.84\times10^{-5}$/K, $\delta = 1$ nm. One can see that during the stage of grain-refinement, an approximate line fitting the plot of $\Delta\alpha_L/\alpha_L^c$ vs. D^{-1} implies that α_L^{nc} is dependent on D. However, when t_m>80 h, a sharp decrease in $\Delta\alpha_L/\alpha_L^c$ was observed, which means a decrease in α_L^{GBs} and/or an increase in α_L^c. α_L^c can be considered as a constant if the lattice structure for the crystallites is assumed unchanged within the stage of D_{min}. So, the observed decrease in $\Delta\alpha_L/\alpha_L^c$ can be attributed to the decrease in α_L^{GBs}. Or in other words, α_L^{GBs} becomes smaller with an extension of ball-milling within D_{min}.

4.2.2. Estimation of the GB enthalpy. The measured stored enthalpy corresponds mainly to the recovery of defects of the milled samples which includes two components simply: non-equilibrium lattice defects in grains and the GBs. The former contribution, for the milled samples, is mainly of the elastic energy of dislocations situated in the grains, and the latter contribution originates mainly from the structural and compositional deviations in the GB region from the inner part of the grains. In plastically deformed materials, the energy of the elastic strain field of the dislocations per unit volume E_{DS} is:

$$E_{DS} = AGb^2\rho \ln(R_e/r_0), \qquad (7)$$

where $A = 1/4\pi$ for screw dislocation and $A = 1/(4\pi(1-\nu))$ for the edge dislocation; here ν is Poisson's ratio and equals 0.291 for Fe [48]. G is the shear modulus, equal to 8.07×10^{10} N/m^2 [49]. R_e and r_0 are the outer and the inner cut-off radii of the dislocations, respectively. In most cases, $r_0 = b$ is taken, R_e, in nc materials, would far exceed D, therefore, D is considered as the outer cut-off radius of the dislocations. The interaction energy of the dislocations can be neglected since, for nc materials, individual grains contain only a few dislocations [20]. Assuming that the grains contain screw and edge dislocations in the same proportion, the constant A must be averaged for the two types of dislocations. Placing the difference between ρ_{milled} and $\rho_{annealed}$ into equation (7), the elastic energy release of the dislocations for the milled Fe after DSC annealing, ΔE_{DS}, can be determined, as plotted in Fig. 12 and listed in Table 1. It can be seen that ΔE_{DS} also possesses a maximum value when $t_m = 80$ h, while it only yields a very small fraction of ΔH, suggesting most of ΔH originates from the GB enthalpy release.

Separating ΔE_{DS} from ΔH, one can get the release of the GB enthalpy, ΔE_{GBs}, as shown in Fig. 12. It can be established that ΔE_{GBs} may yield a dominant part (80–90%) in ΔH. The atoms at GBs may have a slightly different coordination number comparable to those in the grain interiors, and the bonds are also distorted [50]. Upon annealing, structural relaxation may first occur in the GB regions where the broken bonds annihilate, releasing the energy stored at the GBs.

When t_m>20 h, D is nearly unchanged after DSC annealing. So, we can only estimate the GB enthalpy release per area $\Delta\gamma_{GBs}$ ($= \gamma_{GBs}^{milled} - \gamma_{GBs}^{annealed}$; γ_{GBS}^{milled} and $\gamma_{GBs}^{annealed}$ are the GB enthalpy values of the as-milled and as-annealed Fe) by correlating ΔE_{GBs} with the total surface of the GBs per mole, as shown in Fig. 12 and listed in Table 1. One can see that, with an increase in t_m, $\Delta\gamma_{GBs}$ decreases in a linear way. Supposing that $\gamma_{GBs}^{annealed}$ of the milled samples are the same, one can deduce that γ_{GBs}^{milled} decreases in a linear relation with the milling proceeding. γ_{GBs}^{milled} of the sample with $t_m = 140$ h decreased by about 0.1 J/m^2 compared to that of the sample milled for 40 h. The decreased GB enthalpy deduced from the present results is in agreement with those results reported in the literature. In the nc Ni–P [51,52] and Se [53] crystallizing from the amorphous state, as

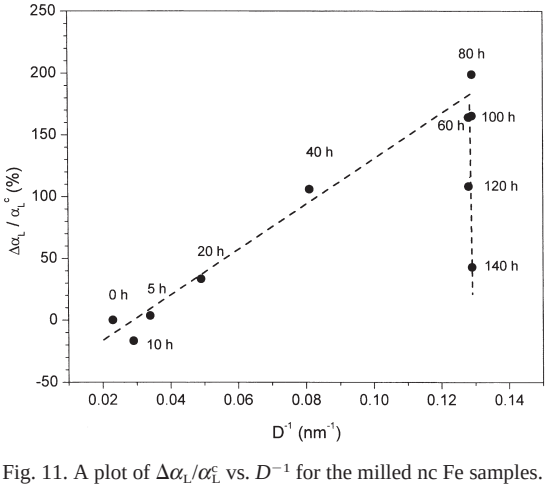

Fig. 11. A plot of $\Delta\alpha_L/\alpha_L^c$ vs. D^{-1} for the milled nc Fe samples.

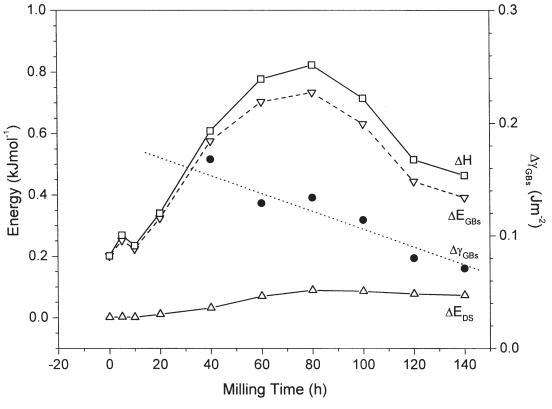

Fig. 12. The stored enthalpy ΔH, the GBs enthalpy release ΔE_{GBs} and the elastic energy release of dislocations ΔE_{DS}, as well as the GB enthalpy release per area $\Delta\gamma_{GBs}$ against the milling time.

well as TiO_2 made by consolidation of ultrafine powders [54], decreases in the GB enthalpy with a reduction in D were observed. The present results, moreover, indicate that even though D remains constant ($t_m \geq 80$ h), the GB enthalpy also decreases with the milling process, which agrees with the decreased ρ_{milled}. Therefore, one can clearly see that further milling of nc Fe at the stage of D_{min} results in a GBs relaxation which causes variations in the structural and thermal properties. By computer simulation, a softening of the GBs in nc materials was also observed [55, 56]. The observed GB relaxation of nc Fe within the stage of D_{min} by milling also highlights one kind of deformation mechanism of the nc materials which needs to be investigated further.

From the above analysis, one can see that the results calculated from XRD and DSC agree well with each other, yielding a common conclusion: GBs are relaxed in the stags of D_{min} by attrition. The results also mean that the XRD Bragg reflections contain a significant contribution from atoms in GBs regions, implying the boundaries in the milled nc Fe are somehow ordered in nature, which would be different from the observations of Zhu *et al.* [57]. This difference may be attributed to the different synthesis procedures of the nc Fe specimens. More accurate characterization of the GB structure in the milled nc Fe will be carried out by using extended X-ray absorption fine-structural spectroscopy (EXAFS) and Mössbauer spectroscopy, in order to understand the nature of the GBs.

5. CONCLUSION

Quantitative XRD and DSC measurement results of the microstructural evolution and thermal properties in nc Fe during mechanical attrition indicated that in the early stages of milling, grain refinement occurs accompanied with an introduction of defects, leading to evident increments of $\langle \varepsilon^2 \rangle^{1/2}$, DWP, α_L^{nc} and ΔH. However, during the stage of D_{min} a slight decrease was found for the structural parameters ($\langle \varepsilon^2 \rangle^{1/2}$ and B_S), and an evident drop in α_L^{nc} and ΔH. This phenomenon can be reasonably interpreted by GB relaxation during mechanical milling, which is supported by clear decreases in α_L^{GBs} and the GB enthalpy. The present work also indicated that the nc materials with D_{min} may exhibit very different properties that depend upon the microstructure of the numerous metastable GBs.

Acknowledgements—Financial support from the Chinese Academy of Sciences, the Max Planck Society of Germany (MPG Partner Group Project), the National Science Foundation of China (grant nos. 59625101 and 59771019) and the Ministry of Science & Technology (G1999064505) is acknowledged.

REFERENCES

1. Gleiter, H., *Prog. Mater. Sci.*, 1989, **33**, 233.
2. Suryanarayana, C., *Int. Mater. Rev.*, 1995, **40**, 41.
3. Lu, K., *Mater. Sci. Engng. Rep.*, 1996, **R16**, 161.
4. Koch, C. C., *Nanostruct. Mater.*, 1993, **2**, 109.
5. Koch, C. C., *Nanostruct. Mater.*, 1997, **9**, 13.
6. Fecht, H. J., in *Nanophase Materials*, ed. G. C. Hadjipanayis and R. W. Siegel. Kluwer Academic Publishers, Netherlands, 1994, p. 125.
7. Fecht, H. J., *Nanostruct. Mater.*, 1995, **6**, 33.
8. Weeber, A. W. and Bakker, H., *Physica*, 1988, **B153**, 93.
9. Eckert, J., Holzer, J. C., Krill III, C. E. and Johnson, W. L., *J. Mater. Res.*, 1992, **7**, 1751.
10. Hellstern, E., Fecht, H. J., Fu, Z. and Johnson, W. L., *J. appl. Phys.*, 1989, **65**, 305.
11. Oleszak, D. and Shingu, P. H., *J. appl. Phys.*, 1996, **79**, 2975.
12. *Powder Diffraction File*, Joint Committee on Powder Diffraction Standards, Swarthmore, PA, 1990, No. 60696.
13. Cox, D. E., Hastings, J. B., Cardoso, L. P. and Finger, L. W., *Mater. Sci. Forum.*, 1986, **9**, 1.
14. Langford, J. I., Delhez, R., Keijser, Th. H. de and Mittemeijer, E. J., Aust. J. Phys., 1988, **41**, 173.
15. Klug, H. P. and Alexander, L. E., *X-ray Diffraction Procedures for Polycrystalline and Amorphous Materials*, 2nd edn. John Wiley and Sons, New York, 1974, chapter 9, p. 491.
16. Bevington, P. R., *Data Reduction and Error Analysis for the Physical Sciences*. McGraw-Hill, New York, 1969.
17. Fecht, H. J., Hellstern, E., Fu, Z. and Johnson, W. L., *Metall. Trans.*, 1990, **A21**, 2333.
18. Malow, T. R. and Koch, C. C., *Acta mater.*, 1997, **45**, 2177.
19. Tian, H. H. and Atzmon, M., *Acta mater.*, 1999, **47**, 1255.
20. Révész, Á., Ungár, T., Borbély, A. and Lendvai, J., *Nanostruct. Mater.*, 1996, **7**, 779.
21. Eastman, J. A., Fitzsimmons, M. R. and Thompson, L. J., *Phil. Mag.*, 1992, **B66**, 667.
22. Zhang, K., Alexandrov, I. V., Valiev, R. Z. and Lu, K., *J appl. Phys.*, 1996, **88**, 5617.
23. Zhao, Y. H. and Lu, K., unpublished.
24. Zhao, Y. H., Zhang, K. and Lu, K., *Phys. Rev.*, 1997, **B56**, 14322.
25. Warren, B. E., *X-ray Diffraction*, Addison-Wesley, Reading, MA, 1969, chapter 11, p. 151.
26. C. H. Macgillavry and G. D. Rieck (ed.) *International Tables for X-ray Crystallography III*. Reidel, Dordrecht, 1983, chapter 3, p. 235.
27. Novotny, V., Holden, T. M. and Dolling, G., *J. Phys.*, 1974, **C52**, 748.
28. Kashiwase, Y., Nishida, I., Kainuma, Y. and Kimoto, K., *J. Phys.*, 1977, **C38**, 2.
29. Ohshima, K., Yatsuya, S. and Harada, J., *J. Phys. Soc. Jpn.*, 1981, **50**, 3071.
30. Minagaki, M., Sasaki, Y. and Sakai, M., *J. Mater. Sci.*, 1983, **18**, 1803.
31. Eastman, J. A. and Fitzsimmons, M. R., *J. appl. Phys.*, 1995, **77**, 522.
32. Harada, J., Yao, S. and Ichimiya, A., *J. Phys. Soc. Jpn.*, 1980, **48**, 1625.
33. Ohahima, K., Yatsuya, S. and Harada, J., *J. Phys. Soc. Jpn.*, 1980, **48**, 1631.
34. Hong, L. B., Ahn, C. C. and Fultz, B., *J. Mater. Res.*, 1995, **10**, 2408.
35. Jiang, J., Ramasamy, S., Birringer, R., Gonser, U. and Gleiter, H., *Solid State Commun.*, 1991, **80**, 525.
36. Zhao, Y. H. and Lu, K., *Phys. Rev.*, 1997, **B56**, 14330.
37. D. E. Gray (ed.) *American Institute of Physics Handbook*, 2nd edn. McGraw-Hill, New York, 1963, chapter 4, p. 66.
38. Birringer, R. and Gleiter, H., in *Advance in Materials Science, Encyclopedia of Materials Science and Engineer-*

ing, ed. R. W. Cahn. Pergamon Press, Oxford, 1988, p. 339.
39. Tong, H. Y., Wang, J. T., Ding, B. Z., Jiang, H. G. and Lu, K., *J. Non-Cryst. Solids*, 1992, **150**, 444.
40. Lu, K. and Sui, M. L., *Acta mater*., 1995, **43**, 3325.
41. Günther, B., Kumpmann, A. and Kunze, H. D., *Scripta metall. mater*., 1992, **27**, 83.
42. Lu, L., Wang, L. B., Ding, B. Z. and Lu, K., *Phil. Mag.*, 2000, in press.
43. Williamson, G. K. and Smallman, R. E., *Phil. Mag*., 1956, **1**, 34.
44. Smallman, R. E. and Westmacott, K. H., *Phil. Mag.*, 1957, **2**, 669.
45. Krivoglaz, M. A., *Theory of X-ray and Thermal-Neutron Scattering by Real Crystals*. Plenum, New York, 1969.
46. Klam, H. J., Hahn, H. and Gleiter, H., *Acta mater*., 1987, **35**, 2101.
47. Qin, X. Y., *Acta phys. Sin.*, 1995, **44**, 244.
48. Nagata, N., Yoshida, S. and Sekino, Y., *Trans. ISIJ*, 1970, **10**, 173.
49. Speich, G. R., Schwoeble, A. J. and Leslie, W. C., *Met. Trans.*, 1972, **3**, 2031.
50. Stern, E. A., Siegel, R. W., Newville, M., Sanders, P. G. and Haskel, D., *Phys. Rev. Lett.*, 1995, **75**, 3874.
51. Lu, K., Lück, R. and Predel, B., *J. Non-Cryst. Solids*, 1993, **156-158**, 589.
52. Lu, K., *Nanostruct. Mater*., 1993, **2**, 643.
53. Lu, K. and Sun, N. X., *Phil. Mag. Lett.*, 1997, **15**, 389.
54. Terwilliger, C. D. and Chiang, Y. M., in *Materials Research Society Symposium Proceedings, Vol. 286*. Materials Research Society, Pittsburgh, PA, 1993, p. 15.
55. Schiøtz, J., Rasmussen, T., Jacobsen, K. W. and Nielsen, O. H., *Phil. Mag. Lett.*, 1996, **74**, 339.
56. Schiøtz, J., Tolla, F. D. Di and Jacobsen, K. W., *Nature*, 1998, **391**, 561.
57. Zhu, X., Birringer, R., Herr, U. and Gleiter, H., *Phys. Rev.*, 1987, **B35**, 9085.